



**HAL**  
open science

## Kinetic modeling of $2e^-/1H^+$ and $2e^-/2H^+$ bidirectional catalytic cycles

Andrea Fasano, Vincent Fourmond, Christophe Léger

► **To cite this version:**

Andrea Fasano, Vincent Fourmond, Christophe Léger. Kinetic modeling of  $2e^-/1H^+$  and  $2e^-/2H^+$  bidirectional catalytic cycles. *Bioelectrochemistry*, 2024, 155, pp.108511. 10.1016/j.bioelechem.2023.108511 . hal-04284492

**HAL Id: hal-04284492**

**<https://hal.science/hal-04284492>**

Submitted on 14 Nov 2023

**HAL** is a multi-disciplinary open access archive for the deposit and dissemination of scientific research documents, whether they are published or not. The documents may come from teaching and research institutions in France or abroad, or from public or private research centers.

L'archive ouverte pluridisciplinaire **HAL**, est destinée au dépôt et à la diffusion de documents scientifiques de niveau recherche, publiés ou non, émanant des établissements d'enseignement et de recherche français ou étrangers, des laboratoires publics ou privés.

# Kinetic modeling of $2e^-/1H^+$ and $2e^-/2H^+$ bidirectional catalytic cycles

Andrea Fasano, Vincent Fourmond and Christophe Léger\*

Laboratoire de Bioénergétique et Ingénierie des Protéines, CNRS, Aix Marseille Université, Marseille, France.

\* [leger@imm.cnrs.fr](mailto:leger@imm.cnrs.fr)

## Abstract

When a redox enzyme or synthetic catalyst is interfaced with an electrode, the electrochemical response depends on the details of the catalytic cycle. Here we focus on the steady-state catalytic waveshape of enzymes such as formate dehydrogenase ( $2e^-/1H^+$ ), hydrogenases ( $2e^-/2H^+$ ) and other bidirectional molecular catalysts that can be adsorbed on, and undergo direct electron transfer with an electrode. We seek to examine the relations between the dependence on pH of the waveshape, the sequence of events in the catalytic cycle, and the properties of the catalytic intermediates (their reduction potentials and  $pK_a$ 's). Discussing the interpretation of the dependence on pH of the limiting currents and catalytic potentials in various simple situations leads us to introduce the concept of "catalytic  $pK_a$ ". The reasoning is general and could be used in relation to any bidirectional two-electron catalytic cycle. Understanding what defines and tunes the catalytic potentials will be crucial for the design of reversible catalysts, which operate at a fast rate in either direction in response to even a small overpotential.

## Keywords

- bidirectional catalysis
- electrochemical kinetics
- protein film voltammetry

## Highlights

- We discuss the shape of bidirectional catalytic voltammograms for molecular catalysts
- Emphasis is on the dependence on pH of catalytic potentials and limiting currents
- This analysis provides a distinct picture from those based on thermodynamics only

## 1. Introduction

When a redox enzyme or a synthetic redox molecular catalyst transfers electrons to/from an electrode, the catalytic process shows up as a catalytic current in a certain potential window. The properties of the catalytic intermediates and the details of the catalytic cycle determine this electrochemical response. Conversely, the magnitude and shape of the catalytic response can be interpreted to gain information about the catalytic cycle [1,2].

In this paper we examine the relation between the mechanism, the thermodynamic and kinetic properties of the catalytic intermediates and the steady-state catalytic response of a two-electron redox catalyst that bidirectionally interconverts substrate and product, under conditions where electron transfer between the catalyst and the electrode is direct. Examples of such catalysts are the enzyme formate dehydrogenase [3] or the  $[\text{Pt}(\text{depe})_2]^{2+}$  catalyst (depe = 1,2-bis(diethylphosphino)ethane) [4] of the two-electron one-proton conversion between  $\text{HCOO}^-$  and  $\text{CO}_2$ , or the enzyme hydrogenase [5] and some of the so-called "Dubois" bioinspired Ni complexes that catalyze the two-electron two-proton oxidation and evolution of  $\text{H}_2$  [6,7].

The theoretical work about two-electron bidirectional catalysis (here and previously in refs [8–11]) contrasts with most of the literature on molecular redox catalysis, which has focussed on *one*-electron models of *unidirectional* catalysis [2,12], with only a few papers describing one-electron models of *bidirectional* catalysis [11,13–17].

We have shown [9] that if the two-electron, bidirectional catalytic mechanism is "ordered" (that is, using the enzymology terminology, the bidirectional catalytic cycle follows a unique sequence of chemical steps clockwise and counterclockwise in the two directions of the reaction), then irrespective of the exact sequence of events in the catalytic cycle, the ideal *steady-state* response has a simple, sigmoidal shape, as shown in figure 1.

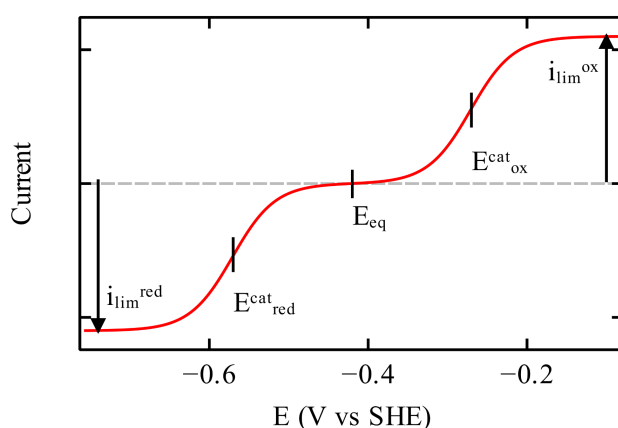


**Figure 1.** The definition of the catalytic potentials and limiting currents, in the generic, ideal catalytic response. The waveshape is plotted here for  $E_{\text{cat}}^{\text{ox}} > E_{\text{cat}}^{\text{red}}$ , and therefore consists of two "one-electron" sigmoids. When  $E_{\text{cat}}^{\text{ox}} < E_{\text{cat}}^{\text{red}}$ , the signal is a unique "two-electron" sigmoid, see e.g. figs 1B and 1C in ref [9].

The current goes from a negative, limiting value at low potential, to a positive, limiting value at high potential. We do not consider any limitation by the transport of substrate towards the electrode, and therefore by assumption, these plateau currents relate to the maximal turnover frequencies in either direction, which are achieved when the rates of oxidation or reduction of the catalyst at the electrode are infinitely fast. The ratio of these two plateau currents is sometimes called the "catalytic

bias". Its value tells whether the catalyst is more active in one direction of the reaction or the other; it is not a thermodynamic quantity [18–20].

The current is zero when the electrode potential equals the equilibrium (Nernst) reduction potential of the substrate/product couple [18]. This equilibrium potential is not a property of the catalyst, and it is a thermodynamic quantity. E.g. for  $H^+/H_2$  conversion [21]:

$$E_{\text{eq}} = E^0 + \frac{RT}{2F} \ln \frac{[H^+]^2}{p_{H_2}} \quad (1)$$

We define the overpotential  $\eta$  in reference to this equilibrium potential:  $\eta = E - E_{\text{eq}}$ . The direction of the reaction only depends on the sign of the overpotential. Note that in contrast, when catalysis is considered unidirectional, either because of the intrinsic properties of the catalyst or because the product of the reaction is not present in the reaction medium, the overpotential is defined in reference to the standard reduction potential of the catalyst [2].

The positions of the steady-state oxidative and reductive sigmoidal waves define two "catalytic potentials",  $E_{\text{cat}}^{\text{ox}}$  and  $E_{\text{cat}}^{\text{red}}$  (figure 1) [8,9], whose interpretation is the main subject of this paper.

Measuring these catalytic potentials requires the analysis of the steady-state catalytic waveshape under conditions where mass transport is not influential. As is the case for non-catalytic voltammetry [22] the two catalytic potentials can only be measured on condition that they are not very crossed (i.e. when  $E_{\text{cat}}^{\text{ox}}$  and  $E_{\text{cat}}^{\text{red}}$  is not too negative), else, the wave shape is essentially a two-electron sigmoid centered on the average value  $(E_{\text{cat}}^{\text{ox}} + E_{\text{cat}}^{\text{red}})/2$ . If interfacial electron transfer is very fast, the two values may be estimated from the inflection points of the oxidative and reductive catalytic waves; if electron transfer is slow and or distributed, the voltammogram is broader and may take an "ohmic" shape, with a linear change in potential against current [8,23]; fitting a model to the wave shape is then required to measure the catalytic potentials, and whether or not the parameters of the models are actually well-defined by the data should be assessed carefully. We have published before programs and procedures that are useful in this context [8,22,24,25].

For an ordered two-electron mechanism, the ratio of limiting currents, the average value of the two catalytic potentials and the equilibrium potential are related by the equation [8,9,24]

$$\frac{i_{\text{lim}}^{\text{ox}}}{i_{\text{lim}}^{\text{red}}} = \exp \left[ \frac{2F}{RT} \left( \frac{E_{\text{cat}}^{\text{ox}} + E_{\text{cat}}^{\text{red}}}{2} - E_{\text{eq}} \right) \right] \quad (2)$$

By our definition of "reversible catalysis" [18], the further apart the two catalytic potentials (the larger the catalytic *overpotentials*), the less reversible the response. If  $E_{\text{cat}}^{\text{ox}}$  is much greater than  $E_{\text{cat}}^{\text{red}}$ , there is a window of electrode potential around  $E_{\text{eq}}$  where no catalysis is observed and the response is termed "irreversible" [25]. If the catalytic potentials are close to one another or even crossed ( $E_{\text{cat}}^{\text{ox}} < E_{\text{cat}}^{\text{red}}$ ), the response shows a single catalytic wave and is termed "reversible", with a current that sharply crosses the X-axis at  $E = E_{\text{eq}}$  and that is significantly negative or positive on either side of  $E_{\text{eq}}$  (see e.g. ref [18] or Box 1 in ref [26]).

The concepts of "catalytic potential" and "catalytic overpotential" ( $\eta_{\text{cat}} = E_{\text{cat}} - E_{\text{eq}}$ ) are only useful when the catalytic cycle includes non-redox chemical steps (as it is often considered in the modeling of molecular catalysts), and thus the catalytic current tends to a plateau at high or low potential, as shown in figure 1. (By "non-redox", we mean that no electron is exchanged with the electrode, and

therefore the rate constants of these transformations are independent of electrode potential.) On the contrary if the catalytic cycle only consists of steps whose rate constants depend on potential (as is often considered in the modeling of surface catalysts), then the current keeps increasing exponentially at high overpotential until mass transport sets a limit, and one is lead to characterize the catalyst by the values of "onset potentials", above which the current becomes greater than a certain arbitrary threshold. Onset potentials cannot be used to evaluate molecular catalysts, because unlike catalytic potentials, their value would depend on the magnitude of the current and therefore on the amount of catalyst (adsorbed on the electrode or added to the solution that bathes the electrode); we do not consider onset potentials further in this paper.

Reversible catalysts are desirable, because they minimize the energy that is dissipated (and wasted) to achieve a fast rate of transformation [18]. It is therefore crucial to understand what defines the catalytic potentials and what makes  $E_{\text{cat}}^{\text{ox}}$  close to or lower than  $E_{\text{cat}}^{\text{red}}$ .

In a previous work [9] we have given the mathematical expressions of the catalytic potentials for various catalytic mechanisms (defined by different orders of the redox and non redox steps). Here we reverse the problem by trying to answer the question of what can be learned about the catalytic cycle by examining the shape and magnitude of voltammograms. Of course very little information can be obtained from a single voltammogram, but here we focus on the variations in waveshape that result from changing the pH. We examine the meaning and pH-dependence of the two catalytic potentials and limiting currents, under various assumptions about the participation of protons in the different steps of the  $2e^-/1H^+$  and  $2e^-/2H^+$  catalytic cycles. Catalytic potentials depart from the equilibrium reduction potentials of the active site [9], and we show here that the change in  $E_{\text{cat}}$  against pH also defines "catalytic  $pK_a$ 's" that are distinct from the true acidity constants defined under equilibrium conditions. We discuss the relations between the Pourbaix diagram of  $E_{\text{cat}}$  against pH, the changes in  $i_{\text{lim}}$  against pH, and the sequence of protonation events in the catalytic cycle.

## 2. Results

We focus on the "EECC" mechanism defined earlier [9], The catalytic cycle consists of two redox steps "E" and two reversible chemical steps "C", as shown in Fig. 2. The active site "A" exists in three redox states (fully oxidized, "O", intermediate, "I", and fully reduced, "R") and the transitions are characterized by two equilibrium reduction potentials  $E_1^0$  and  $E_2^0$  (for the O/I and I/R couples, respectively). The two bidirectional chemical steps have pseudo first order rate constants  $k_1$ ,  $k_{-1}$ ,  $k_2$ ,  $k_{-2}$  (the positive subscripts correspond to the direction of reductive catalysis, e.g.  $H_2$  evolution). These two steps may correspond to substrate/product binding and release, or to intramolecular transformations (e.g.  $H_2$  splitting, intramolecular proton or hydride transfers etc.). In this paper we assume that the redox steps are infinitely fast (this is the "Nernstian limit"), so that O, I and R equilibrate with the electrode even under conditions of turnover. However, the model does not assume that the "E" steps are *pure* electron transfers, they may be coupled to chemical reactions that are fast on the time scale of catalysis.

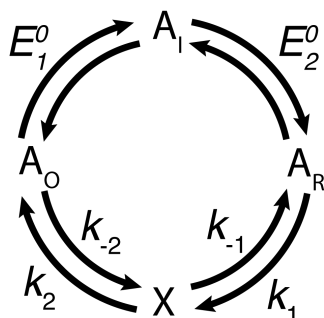


**Figure 2** The scheme of the catalytic mechanism EECC<sup>1</sup>. A<sub>O</sub>, A<sub>I</sub> and A<sub>R</sub> are the oxidized, intermediate, and reduced forms of the active site. X is a catalytic intermediate. All steps are reversible.

In ref [9], we gave the expressions of the limiting currents and of the catalytic potentials defined in fig. 1 as a function of the parameters of the model in fig. 2 ( $E_1^0, E_2^0, k_1, k_2, k_{-1}, k_{-2}$ ) without making any assumption about the protonation pattern and the pH dependence of these parameters:

$$E_{\text{cat}}^{\text{ox}} = E_1^0 - \frac{RT}{F} \ln \frac{k_2 + k_{-1} + k_{-2}}{k_2 + k_{-1}} \quad (3)$$

$$E_{\text{cat}}^{\text{red}} = E_2^0 + \frac{RT}{F} \ln \frac{k_2 + k_{-1} + k_1}{k_2 + k_{-1}} \quad (4)$$

Eqs 3 and 4 are only valid for an heterogenized molecular catalyst. Different equations apply if the catalyst diffuses in solution to/from the electrode [9]. The catalytic potentials depart from the reduction potentials of the active site, and the larger  $k_1 k_2 / k_{-1} k_{-2}$  (that is, the more stable the intermediate "X" between the two C steps), the closer the two catalytic potentials and the more reversible the response [9].

At high or low potential, the redox steps are infinitely fast, and the catalytic current tends to limiting values which only depend on the values of the rate constants of the C-steps. Again for an heterogenized catalyst:

$$i_{\text{lim}}^{\text{ox}} = 2FA\Gamma \frac{k_{-1} k_{-2}}{k_2 + k_{-1} + k_{-2}} \quad (5)$$

$$i_{\text{lim}}^{\text{red}} = -2FA\Gamma \frac{k_1 k_2}{k_1 + k_2 + k_{-1}} \quad (6)$$

These equations remain valid for a unidirectional reaction, which occurs when at least one of the rate constants of the chemical steps is zero.

To discuss the variations of the catalytic response (catalytic potentials, limiting currents) with pH, we need to explicitly designate which steps of the EECC cycle are or include the (de)protonations (intermolecular proton transfers). This leads us to define various cases below. We may for example assume that a particular redox step is coupled to a protonation that is so **fast** that it remains at equilibrium even on the catalytic time scale. (The expression "coupling" here, as in "proton coupled electron transfer", implies that under equilibrium conditions, a protonation occurs upon reduction,

without assuming that the mechanism is stepwise (either proton first or electron first) or concerted [27,28]). The effect of this *fast* proton transfer is to make the reduction potentials  $E_1^0$  or  $E_2^0$  depend on pH, but the rate constants of (de)protonation do not appear in the model. We may also assume that one particular C step includes a protonation by explicitly assuming a pH dependence of the forward and backward pseudo-first-order rate constants.

For the sake of simplicity, we shall assume that the slow intermolecular protonation steps occur with a pseudo-first order rate constant proportional to  $[H^+]$ , whereas deprotonation rate constants are independent of pH. Different results would have been obtained under the assumption that the deprotonation rate constant is proportional to  $[OH^-]$ , or if we considered the kinetics of proton transfer to/from a weak acid in solution or a proton transfer relay in the enzyme. The latter, more general hypothesis is discussed at the end of this paper. However, the simple assumptions used here are useful to introduce important and general concepts that remain valid irrespective of the details of the (de)protonation kinetics.

## 2.1 Two-electron one-proton

We first discuss two-electron one-proton catalytic cycles, like that for the conversion of formate and  $CO_2$ .

	1	2	3	4	5
$E_1^0$	—		—		
$E_2^0$		—	—		
$k_1$				$H^+$	
$k_2$					$H^+$

Table 1: Five possible manners to include 1 intermolecular protonation event into the four-step EECC catalytic cycle. When the protonation step is fast, it is shown in the table as a slanted line, to represent the  $-60 \text{ mV/pH}$  dependence of the reduction potential. An " $H^+$ " in the rows labeled  $k_1$  or  $k_2$  means that a bimolecular protonation occurs in the first or the second chemical step, respectively.

For the sake of completeness, we consider the 5 possible protonation patterns depicted in Table 1, where each line corresponds to one of the 4 steps in the EECC catalytic cycle. The implication of protons in certain steps is indicated by symbols (a slanted line or a " $H^+$ ") in each cell of the table, and by colors in the round schemes in each column.

We consider the cases where the protonation is fast (at equilibrium) and coupled to the 1<sup>st</sup> (case 1) or 2<sup>nd</sup> (case 2) reduction of the active site, or to the 1<sup>st</sup> reduction when pH < pK and to the second reduction when pH > pK (case 3), or the protonation occurs in the 1<sup>st</sup> (case 4) or 2<sup>nd</sup> (case 5) chemical step.

When the protonation step is fast, it is shown in the table as a slanting line, to represent the -60 mV/pH dependence of the reduction potential. An "H<sup>+</sup>" in the rows labeled  $k_1$  or  $k_2$  means that a bimolecular protonation occurs in the first or the second chemical step, respectively. We also use circular schemes where a red arrow indicates a protonation in a E or C step, and two orange arrows are used to symbolize the single, fast protonation occurring in the 1st or 2nd step depending on pH (case 3).

We shall discuss the physical meaning of the observables (the pH dependence of the catalytic potentials and the catalytic currents in both directions) to derive the rules that can be used to qualitatively interpret the voltammetry in relation to the series of events that take place in the catalytic cycle.

Table 2 contains the equations of the catalytic potentials and limiting currents as a function of pH in each of the 5 cases. These equations are plotted in Fig. 3. All curves are arbitrarily offset along the Y axis, since only the variations with pH are discussed here.

**Cases 1 and 2.** In cases 1 and 2 (table 1), the (de)protonation step is assumed to be coupled to the 1<sup>st</sup> or 2<sup>nd</sup> reduction of the active site, respectively (from O to I, or from I to R) and fast on the catalytic time scale (therefore at equilibrium). The reductive catalytic cycle is completed by two steps that are neither electron transfers nor intermolecular proton transfers. Therefore either one reduction potential or the other decreases linearly with pH, while the other is pH-independent:

In case 1

$$E_1^{0'} = E_1^0 - 2.3 \frac{RT}{F} \times pH \quad (7)$$

and in case 2

$$E_2^{0'} = E_2^0 - 2.3 \frac{RT}{F} \times pH \quad (8)$$

The expressions of the catalytic potentials are given in table 2 and plotted in fig. 3. The pH-dependences of the two catalytic potentials are merely the same as those of the two reduction potentials of the active site. The two catalytic potentials are shifted from the two  $E^0$ 's by an amount that depends on the pH-independent values of the four rate constants  $k_1, k_{-1}, k_2, k_{-2}$  (cf eqs 3 and 4). Reversibility (with  $E_{cat}^{ox} - E_{cat}^{red}$  small or even negative) is achieved at high pH in case 1 and low pH in case 2.

The values of the two limiting currents, which define the magnitude of the low- and high potential plateau currents, only depend on  $k_1, k_{-1}, k_2, k_{-2}$  (table 2, cf eqs 5 and 6) and are thus pH independent, as shown in fig. 3.

**Case 3** is a generalization of cases 1 and 2: we note "pK" the pK<sub>a</sub> of the half reduced form of the active site (I), so that case 1 and 2 are recovered when the pH is lower or greater than pK. Again the

pH dependence of the catalytic potential matches that of the two redox potentials of the active site, and the two limiting currents are pH independent. The greater reversibility is achieved at  $\text{pH}=\text{p}K$  (where  $E_{\text{cat}}^{\text{ox}}-E_{\text{cat}}^{\text{red}}$  takes the smallest value).

In cases 1-3, the dependence on pH of the two catalytic potentials clearly indicates whether or not the redox steps are coupled to a protonation (which, by assumption, remains at equilibrium). And the fact that both  $i_{\text{lim}}^{\text{ox}}$  and  $i_{\text{lim}}^{\text{red}}$  are pH independent is consistent with both slow, bidirectional chemical steps being pH-independent.

**Case 4.** The protonation step follows the 2<sup>nd</sup> electron transfer step, but in contrast to the fast coupling case 2, it is now allowed to be slow on the time scale of turnover. This is the putative mechanism of the Pt(depe)<sub>2</sub> complex according to ref [4], with the second, composite step including a series of pH-independent chemical events (formate binding, hydride transfer and CO<sub>2</sub> release).

The reduction potentials of the active site are pH independent and we assume that the protonation in the 1<sup>st</sup> C-step occurs with a bimolecular rate constant  $k'_1$

$$k_1 = k'_1 \times [\text{H}^+] \quad (9)$$

whereas  $k_{-1}$ ,  $k_2$  and  $k_{-2}$  remain pH-independent.

The reductive limiting current is limited by the two C steps, and follows Michaelis-Menten kinetics (considering that the proton is a substrate), with a maximal rate that is proportional to  $k_2$ :

$$i_{\text{lim}}^{\text{red}} = -2FA\Gamma \frac{k_2}{1 + \frac{K_c}{[\text{H}^+]}} \quad (10)$$

The apparent acidity constant  $K_c$  departs from the true acidity constant  $k_{-1}/k'_1$  all the more than  $k_2$  is large:

$$K_c = \frac{k_2 + k_{-1}}{k'_1} \quad (11)$$

This departure between true and apparent acidity constant is typical of the Briggs-Haldane version of the Michaelis-Menten equation [29,30]. Such "catalytic  $\text{p}K_c$ 's" will appear in many of the equations in this work.

The oxidative limiting current is pH independent, because under very oxidizing conditions the forward oxidation of the fully reduced active site (R to I) is so fast that it outcompetes its backward protonation (R to X), so that the value of the pH-dependent protonation rate constant  $k_1$  does not affect the oxidative limiting current.

$E_{\text{cat}}^{\text{ox}}$  is pH-independent and the pH dependence of  $E_{\text{cat}}^{\text{red}}$  reveals the protonation that follows the 2<sup>nd</sup> reduction (I to R), in the 1<sup>st</sup> C step. Under equilibrium conditions, this protonation would occur at  $\text{pH} < -\log_{10}(k_{-1}/k'_1)$ , but under steady-state catalytic conditions, the dependence of  $E_{\text{cat}}^{\text{red}}$  on pH defines an apparent acidity constant  $K_c$  that is the same as that derived from the michaelian change in  $i_{\text{lim}}^{\text{red}}$  against  $[\text{H}^+]$ :

$$E_{\text{cat}}^{\text{red}} = E_2^0 + \frac{RT}{F} \ln \left( 1 + \frac{[\text{H}^+]}{K_c} \right) \quad (12)$$

Despite the fact that in the reductive catalytic cycle, the 2<sup>nd</sup> reduction is immediately followed by a protonation, only at low pH does the pH dependence of  $E_{\text{cat}}^{\text{red}}$  reveal that protonation. At pH above

$pK_c$ , this protonation becomes slow (compared to  $k_2 + k_{-1}$ , and indeed, the reductive limiting current decreases one decade per pH-unit), and  $E_{cat}^{red}$  becomes pH independent.

**Case 5.** The protonation occurs in the second C-step, so that  $k_1$  is pH-independent, and

$$k_2 = k'_2[H^+] \quad (13)$$

The change in  $i_{lim}^{red}$  with pH is Michaelian, like in cases 4, but with a maximal value proportional to  $k_1$ , and an apparent acidity constant that is *not* related to any acidity constant:

$$K_c = \frac{k_{-1} + k_1}{k'_2} \quad (14)$$

In contrast to case 4,  $i_{lim}^{ox}$  is pH dependent:

$$i_{lim}^{ox} = 2FA\Gamma \frac{\frac{k_{-1}k_{-2}}{k_{-1}+k_{-2}}}{1 + \frac{[H^+]}{K_b}} \quad (15)$$

$i_{lim}^{ox}$  decreases at low pH when the backward protonation step 2 (X to O) outcompetes the forward step -1 (X to R). This results in product inhibition of oxidative catalysis, with an inhibition constant  $K_b$  which departs from the true acidity constant  $k_2/k'_2$ :

$$K_b = \frac{k_{-1} + k_{-2}}{k'_2} \quad (16)$$

The values of  $pK_c$  and  $pK_b$  also influence  $E_{cat}^{ox}$  and  $E_{cat}^{red}$ . At  $pH < pK_b$  (that is,  $k'_2[H^+] > k_{-1}+k_{-2}$ ), where protons inhibit oxidative catalysis by preventing the forward deprotonation step "-2" (O to X),  $E_{cat}^{ox}$  is pH-independent like  $E^0_1$ . At higher pH ( $pK_e > pH > pK_b$ ; with  $K_e = k_{-1}/k'_2$  as defined in Table 2), the deprotonation in step -2 makes the pH dependence of  $E_{cat}^{ox}$  60mV/pH more negative than that of  $E^0_1$  (-60mV/pH) on condition that  $pK_e > pK_b$  (that is  $k_{-2} > k_{-1}$ ). In contrast, if  $k_{-2} < k_{-1}$  ( $pK_e = pK_b$ ), the deprotonation in step -2 at  $pH > pK_b$  does not affect the pH dependence of  $E_{cat}^{ox}$  because the "X" intermediate is not stable, and the fully reduced state R accumulates. Similarly,  $E_{cat}^{red}$  depends on pH only if  $pK_e > pK_c$  (that is  $k_1 > k_{-1}$ ). It increases with pH to reach the value  $E^0_2 + RT/F \log(1+k_1/k_{-1})$  at  $pH > pK_e$ . This high-pH limit reflects the equilibrium between  $A_i$ ,  $A_R$  and X. Instead, if  $pK_e = pK_c$  (that is  $k_1 < k_{-1}$ ),  $E_{cat}^{red}$  is pH independent.

Note that Case 5 illustrates a situation where  $E_{cat}^{red}$  may increase as the pH increases, but the average two electron potential  $(E_{cat}^{ox} + E_{cat}^{red})/2$  necessarily decreases as the pH increases, consistent with catalysis being increasingly biased in the direction of proton reduction (eq 2).

This increase in  $E_{cat}^{red}$  with pH certainly does *not* imply that a reduction is followed by a deprotonation in the catalytic cycle. This shows that the Pourbaix diagram of  $E_{cat}$  cannot be simply analyzed to obtain the protonation pattern.

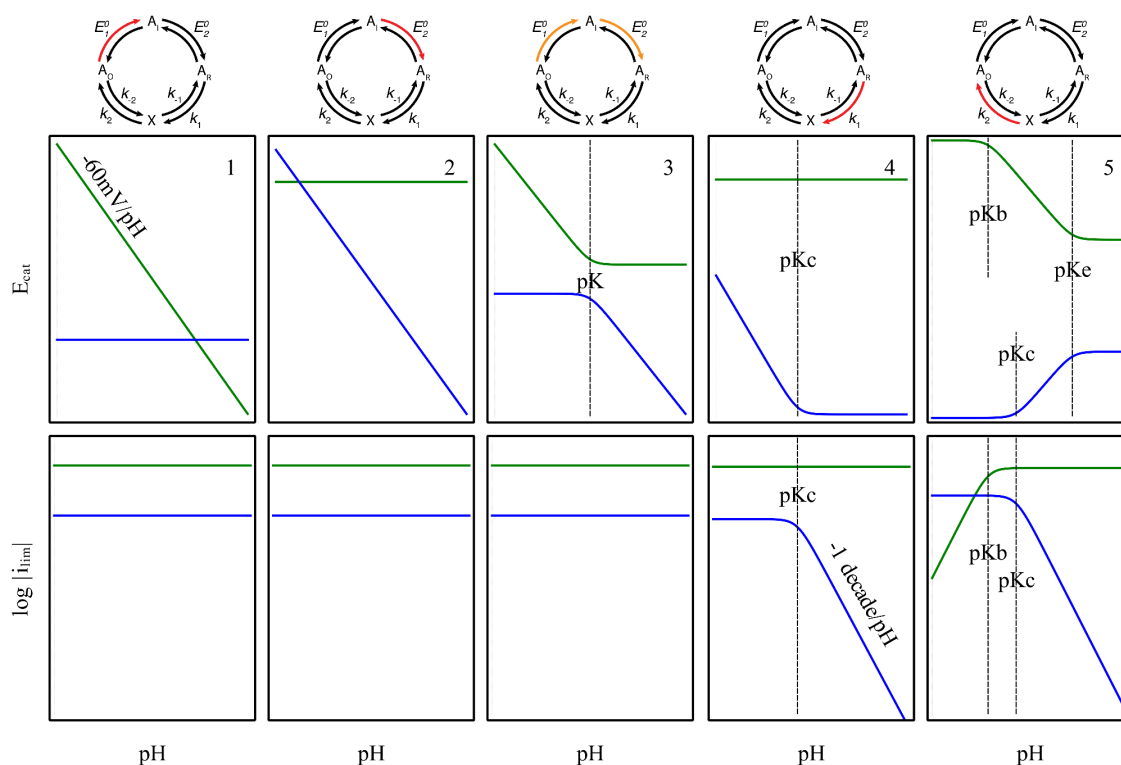


**Figure 3.** The catalytic potentials and the logarithm of the limiting currents as a function of pH for all cases described in table 1.  $E_{\text{cat}}^{\text{ox}}$  and  $i_{\text{lim}}^{\text{ox}}$  are in green;  $E_{\text{cat}}^{\text{red}}$  and  $i_{\text{lim}}^{\text{red}}$  in blue. The vertical dash lines mark the values of each catalytic  $\text{p}K_a$ . In cases 3, 4 and 5 those lines run through the entire panel when that  $\text{p}K$  influences both catalytic potentials, whereas they are interrupted if they influence only one of the two potentials. On top the circular schemes of protonation pathways used in table 1 are reported per each case.

Case	$E_{\text{cat}}^{\text{ox}}$	$i_{\text{lim}}^{\text{ox}}$	$E_{\text{cat}}^{\text{red}}$	$i_{\text{lim}}^{\text{red}}$	
1	$E_1^0 - 2.3 \frac{RT}{F} \times pH - \frac{RT}{F} \ln \frac{k_2 + k_{-1} + k_{-2}}{k_2 + k_{-1}}$	$2FA\Gamma \frac{k_{-1}k_{-2}}{k_2 + k_{-1} + k_{-2}}$	$E_2^0 + \frac{RT}{F} \ln \frac{k_2 + k_{-1} + k_1}{k_2 + k_{-1}}$	$-2FA\Gamma \frac{k_1k_2}{k_1 + k_2 + k_{-1}}$	
2	$E_1^0 - \frac{RT}{F} \ln \frac{k_2 + k_{-1} + k_{-2}}{k_2 + k_{-1}}$		$E_2^0 - 2.3 \frac{RT}{F} \times pH + \frac{RT}{F} \ln \frac{k_2 + k_{-1} + k_1}{k_2 + k_{-1}}$		
3	$E_1^0 + \frac{RT}{F} \ln \left[ 1 + \frac{[H^+]}{K} \right] - \frac{RT}{F} \ln \frac{k_2 + k_{-1} + k_{-2}}{k_2 + k_{-1}}$		$E_2^0 - \frac{RT}{F} \ln \left[ 1 + \frac{K}{[H^+]} \right] + \frac{RT}{F} \ln \frac{k_2 + k_{-1} + k_1}{k_2 + k_{-1}}$		
4	$E_1^0 - \frac{RT}{F} \ln \frac{k_2 + k_{-1} + k_{-2}}{k_2 + k_{-1}}$		$E_2^0 + \frac{RT}{F} \ln \left[ 1 + \frac{[H^+]}{K_c} \right]$	$-2FA\Gamma \frac{k_2}{1 + \frac{K_c}{[H^+]}}$	$K_c = \frac{k_2 + k_{-1}}{k_1'}$
5	$E_1^0 + \frac{RT}{F} \ln \frac{1 + \frac{[H^+]}{K_c}}{1 + \frac{[U]}{K_b}} + \frac{RT}{F} \ln \frac{K_c}{K_b}$	$2FA\Gamma \frac{k_{-1}k_{-2}}{1 + \frac{[U]}{K_b}}$	$E_2^0 + \frac{RT}{F} \ln \frac{1 + \frac{[U]}{K_c}}{1 + \frac{[H^+]}{K_c}} + \frac{RT}{F} \ln \frac{K_c}{K_c}$	$-2FA\Gamma \frac{k_1}{1 + \frac{K_c}{[H^+]}}$	$K_e = \frac{k_{-1}}{k_2'}$ $K_b = \frac{k_{-1} + k_{-2}}{k_2'}$ $K_c = \frac{k_{-1} + k_1}{k_2'}$

Table 2 The pH dependence of the catalytic potentials and the limiting currents for each of the 5  $2e^-/1H^+$  cases described in table 1.

## 2.2 Two-electron two-proton

We now consider a two-electron two-proton reaction, like the  $2\text{H}^+/\text{H}_2$  conversion. Two of the four steps of the catalytic cycle must include a (de)protonation. The various possibilities define 8 distinct protonation patterns, listed in table 3, each of which corresponds to a distinct assumption regarding which of the 4 steps include a protonation and depend on pH.

Table 4 gives the equations of the catalytic potentials and limiting currents as a function of pH in each of the 8 cases. The equations are plotted in Fig. 4.

**Case 1** corresponds to the situation where each of the two (de)protonation steps is fast on the time scale of turnover (therefore it remains at equilibrium), and coupled to an electron transfer. Therefore both standard reduction potentials decrease linearly with pH

$$E_1^{0'} = E_1^0 - 2.3 \frac{RT}{F} \times \text{pH} \quad (17)$$

and

$$E_2^{0'} = E_2^0 - 2.3 \frac{RT}{F} \times \text{pH} \quad (18)$$

The two "C" steps do not include any (de)protonation and therefore the corresponding rate constants are pH-independent.

case	1	2	3	4	5	6	7	8
$E_1^0$								
$E_2^0$								
$k_1$		$\text{H}^+$	$\text{H}^+$	$\text{H}^+$				$\text{H}^+$
$k_2$					$\text{H}^+$	$\text{H}^+$	$\text{H}^+$	$\text{H}^+$

Table 3: Eight possible ways to include 2 intermolecular protonation steps into the four-step EECC catalytic cycle. When the protonation step is fast and coupled to an electron transfer step, it is shown in the table as a slanting line, to represent the  $-60 \text{ mV/pH}$  dependence of the reduction potential. An " $\text{H}^+$ " in the rows labeled  $k_1$  or  $k_2$  means a protonation occurs in the first or the second chemical step, respectively.

Under this assumption, the two catalytic potentials decrease 60 mV per pH unit, like  $E_1^{\text{ox}}$  and  $E_2^{\text{ox}}$ , but are offset from the true reduction potentials (as per eqs 3 and 4).

Here, as shown in fig. 4, panel 1, the dependence on pH of the two catalytic potentials clearly indicates the coupling of each redox step with a fast protonation (which remains at equilibrium). And the fact that both  $i_{\text{lim}}^{\text{ox}}$  and  $i_{\text{lim}}^{\text{red}}$  are pH independent is consistent with both bidirectional chemical steps being pH-independent. This situation is similar to the cases 1 to 3 in Fig. 3.

Regarding **cases 2, 3 and 4**, we assume that the two-electron reduction of the active site is coupled to only one *fast* protonation, the second protonation is bimolecular and occurs in the 1<sup>st</sup> C step, and only  $k_1$  is pH dependent:

$$k_1 = k'_1 \times [\text{H}^+] \quad (19)$$

As for  $2e^-/1\text{H}^+$  case 4 above, the 2<sup>nd</sup> reduction and the 2<sup>nd</sup> protonation are coupled and occur in a stepwise manner (electron first, proton second).

In **case 2**, the 1<sup>st</sup> reduction is coupled to a fast protonation, and the 2<sup>nd</sup> is pH-independent. The situation is very similar to the  $2e^-/1\text{H}^+$  case 4 above. The reductive limiting current follows Michaelis-Menten kinetics with an apparent acidity constant  $K_c$  that departs from the true acidity constant, and the oxidative limiting current is pH independent.

$E_{\text{cat}}^{\text{ox}}$  decreases 60mV/pH, like  $E_1^{\text{ox}}$ , and the pH dependence of  $E_{\text{cat}}^{\text{red}}$  reveals the protonation in the 1<sup>st</sup> C step, after full reduction, and defines an apparent acidity constant  $K_c$  that is the same as that observed in the michaelian change in  $i_{\text{lim}}^{\text{red}}$  against  $[\text{H}^+]$ .

Only at low pH does the pH dependence of  $E_{\text{cat}}^{\text{red}}$  reveal the protonation event in the 1<sup>st</sup> C step. At pH above  $\text{p}K_c$ , this protonation becomes slow (compared to  $k_2 + k_{-1}$ , and indeed, the reductive limiting current decreases one decade per pH-unit), and  $E_{\text{cat}}^{\text{red}}$  becomes pH independent.

In **case 3**, we assume that the 2<sup>nd</sup> reduction is coupled to a fast protonation, and the second protonation still occurs in the 1<sup>st</sup> C step (with a second order rate constant  $k'_1$ ).

The changes in limiting current against pH (or absence thereof) are the same as those in case 2. The fact that  $E_{\text{cat}}^{\text{ox}}$  is pH-independent reveals the absence of protonation coupled to the 1<sup>st</sup> redox step. Like in case 2, the dependence on pH of  $E_{\text{cat}}^{\text{red}}$  reveals the number of protonation steps that go with the 2<sup>nd</sup> reduction *and are fast*: only one proton at  $\text{pH} > \text{p}K_c$  when one of the two protonation steps is slow ( $k'_1[\text{H}^+] < k_2 + k_{-1}$ ) and limits reductive turnover (hence the decrease in reductive current at high pH); and two protons at  $\text{pH} < \text{p}K_c$ , when the rate of protonation  $k'_1[\text{H}^+]$  is fast compared to  $k_2 + k_{-1}$ .

**Case 4** is more general than cases 2 and 3: here we assume that the half reduced active site quickly (de)protonates with a certain equilibrium acidity constant ( $K$ ). This assumption gives back either case 2 or case 3 if  $\text{p}K$  is large or small, respectively.

In case 4, the changes in  $E_{\text{cat}}$  against pH define two different acidity constants, one is the true  $\text{p}K$  of the half reduced active site, and the other,  $\text{p}K_c$  defined above, is dependent on kinetics. In Fig. 4, panel 4 shows two possible dependences of  $E_{\text{cat}}^{\text{red}}$  on pH, depending on whether  $\text{p}K_c < \text{p}K$  (light blue line) or  $\text{p}K_c > \text{p}K$  (dark blue line).

The pH dependence of the reductive limiting current reveals the presence of a protonation step that is rate limiting at pH greater than  $pK_c$ , but the value of  $pK$  (the acidity constant of the half reduced state) does not influence the change in limiting currents against pH. This is because the limiting currents are determined by the rate constants of the C-steps (eqs 5 and 6), and are not affected by the fast reactions that may be coupled to the E steps.

Case	$E_{cat}^{ox}$	$i_{lim}^{ox}$	$E_{cat}^{red}$	$i_{lim}^{red}$	$K_c$
1					

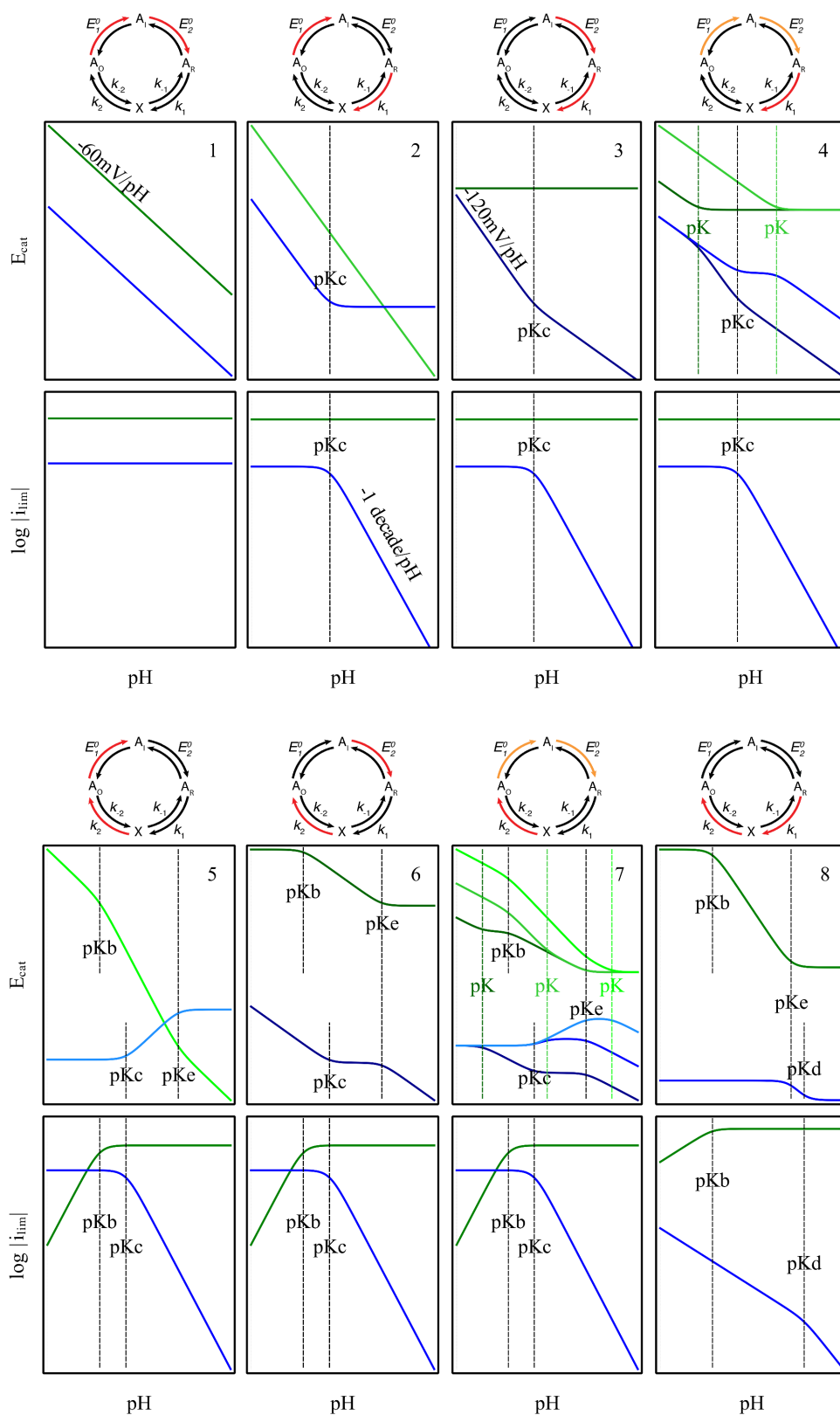


**Figure 4.** The catalytic potentials and the logarithm of the limiting currents for all  $2e^-/2H^+$  cases described in table 3.  $E_{cat}^{ox}$  and  $i_{lim}^{ox}$  are in green;  $E_{cat}^{red}$  and  $i_{lim}^{red}$  in blue. The vertical dash lines mark the values of each catalytic pK. In panels 5, 6, 7 and 8 those lines run through the entire panel when that pK influences both catalytic potentials, whereas they are interrupted if they influence only one of

the two potentials. Panel 4 and 7 represent the general cases in which one protonation occurs in the first or the second chemical step respectively, and the other is coupled to the first or the second redox step depending on whether the pH is lower or greater than  $pK$ , respectively. Different possible values of that  $pK$  are represented with green or blue shades, the darker the lower the value. The circular schemes of protonation pathways used in table 3 are shown on top.

**Cases 5, 6 and 7** mirror cases 2,3 and 4, with the protonation now occurring in the second C-step, so that  $k_1$  is pH-independent, and  $k_2 = k_2' [H^+]$ . The situation is similar to the  $2e^-/1H^+$  case 5, but the pH dependence of the  $E^0$  of the 1<sup>st</sup> or 2<sup>nd</sup> E step adds a pH-dependence to the catalytic potentials. Here in cases 5 and 6, the 1<sup>st</sup> or 2<sup>nd</sup> redox steps are coupled to a fast protonation respectively. In case 7, the half-reduced active site protonates at  $pH < pK$ . From case 7, the limiting situations where  $pK$  is large or small give back cases 5 and 6, respectively. As an example, we explain in the supplementary information the derivation of the pH dependence of the catalytic potentials in case 5.

In all three cases, the change in  $i_{lim}^{red}$  against pH is Michaelian, with an apparent acidity constant  $K_c$ , and  $i_{lim}^{ox}$  decreases at low pH, below  $pK_b$ .

The values of  $pK_c$  and  $pK_b$  influence  $E_{cat}^{ox}$  and  $E_{cat}^{red}$  as discussed for the  $2e^-/1H^+$  case 5, and, again, the increase in  $E_{cat}^{red}$  with pH does *not* imply that a reduction is coupled to *deprotonation* in the catalytic cycle.

**Case 8.** Last, we consider the situation where the two protonations occur in the C steps, with second order rate constants  $k'_1$  and  $k'_2$ . The variations with pH of the limiting currents and catalytic potentials define 4 apparent acidity constants,  $K_e$ ,  $K_b$ ,  $K_c$ ,  $K_d$ , none of which is an equilibrium constant. The meaning of  $pK_b$  and  $pK_e$  is the same as before.

It is the only case where the reductive limiting current does not follow Michaelis Menten kinetics (there is no maximal rate at low pH), and the reductive current may change two decades per pH unit ; this occurs when  $pH > pK_d$ , that is  $[H^+] > k_{-1}/(k'_2+k'_1)$ .

### 3. Discussion

In an approach based on the thermodynamic modeling of the catalytic cycle, the sequence of events is deduced from the interpretation of Pourbaix diagrams of the dependence on pH of the redox reduction potential of the active site of hydrogenase[31]. In ref [32] for example, the reduction potentials of the active site of *C. reinhardtii* FeFe hydrogenase were measured as a function of pH, and discussed under the assumption that they are relevant to the catalytic cycle. In this approach, the reduction potentials of the active site and the catalytic potentials are implicitly assumed to be the same. For example,[31] a very efficient (i.e. reversible) enzyme like hydrogenase is said to be optimized by Nature so that two equilibrium redox potentials of the active site are "as close as possible" to  $E_{eq}$ .

Kinetic modeling gives a different picture.

In ref [9], we have examined various ordered two-electron catalytic mechanisms (each defined by a particular sequence of redox and chemical steps), we have calculated the steady-state

electrochemical responses (both for diffusing and adsorbed redox catalysts), and we have shown that in the general case, the shape of the steady-state catalytic voltammogram defines two "catalytic potentials", which depart from the reduction potentials of the active site. Just like Michaelis constants are apparent dissociation constants, the catalytic potentials, whose values define the (ir)reversibility of the catalytic response, are *kinetic* parameters.

Here, we have explored and discussed the pH dependence of the steady-state catalytic response of an adsorbed catalyst in the framework of an "EECC" catalytic cycle, considering 13 distinct options regarding the possible protonation patterns. We have considered protonation steps fast and coupled to the redox (E) steps (thus at equilibrium), or occurring in the chemical (C) steps, with second-order kinetics, and we discussed the effect of pH on magnitude and shape of the catalytic voltammograms. These considerations apply to any two-electron catalytic transformation between a substrate and a product, with substrate and product binding/release occurring in any of the four steps. The calculations could be extended to discuss the effect of changing the concentration of product (e.g. H<sub>2</sub>) on the catalytic response, or using different assumptions about the proton transfer kinetics (here for the sake of simplicity we have assumed bimolecular protonation kinetics).

In the Pt(depe)<sub>2</sub> catalytic cycle of CO<sub>2</sub>/formate conversion, the cooperative two-electron reduction of the Pt ion is followed by a slow protonation, and then by hydride transfer[4]. This can be described by an EECC mechanism, where the rate constant of the 1<sup>st</sup> C-step would depend on pH (this is the 2e<sup>-</sup>/1H<sup>+</sup> case 4). In *Bacillus subtilis* ForCE 1 formate dehydrogenase, the second reduction of the active site Mo ion (Mo<sup>V</sup> to Mo<sup>IV</sup>) is coupled to a fast protonation [3] (this is case 2). In *D. vulgaris* FdhAB formate dehydrogenase, the half-reduced active site (Mo<sup>V</sup>) protonates with a pK<sub>a</sub> around 6.5 [3] (case 3).

A first goal, reached in the results section, was to deduce the change in waveshape with pH (catalytic potentials and limiting currents) for each possible mechanism and protonation scenario. In a reverse engineering approach, the more challenging goal is to understand whether, and how, the details of the catalytic cycle can be elucidated from the variations with pH of  $E_{cat}$  and  $i_{lim}$ , as exemplified recently in our voltammetric study of the catalytic mechanism of formate dehydrogenase adsorbed onto a rotating electrode[3].

As shown in Fig. 3 and Fig. 4, each case that we have considered implies a distinct pH dependence of the catalytic potentials and the limiting currents. So, at least on paper, it should be possible to distinguish the mechanism based on the experimental information. However, very different protonation patterns may give, in a limited pH range, the same pH dependences. Compare for example the 2e<sup>-</sup>/2H<sup>+</sup> case 2 and the 2e<sup>-</sup>/2H<sup>+</sup> case 6 in the pH range pK<sub>b</sub> < pH < pK<sub>c</sub>. This indicates that the interpretation of Pourbaix diagrams of  $E_{cat}$  might not always be straightforward. The dependence of the catalytic potentials on pH *alone* is not always enough to elucidate the sequence of electron and proton transfers in the catalytic cycle. Its combination with the pH dependence of the limiting currents surely helps in the discrimination of different sequences of catalytic steps, even though it might not be sufficient if the experimental pH range is narrow.

## 4. Conclusions and perspectives

We have examined the catalytic response of an adsorbed catalyst of two-electron reactions, in the framework of an ordered, bidirectional, four-step catalytic cycle. This analysis tells us that the observed dependence on pH of the catalytic potentials and of the limiting currents reached at very high and very low electrode potentials define "catalytic  $pK_a$ 's", which are not true acidity constants, just like a Michaelis constant is not a true dissociation constant [29]. The deviations from true equilibrium constant implies that the Pourbaix diagrams of  $E_{\text{cat}}$  cannot be used to deduce the acidity constants of the intermediates, and that the latter, which may be determined under equilibrium conditions, are not necessarily relevant to catalysis.

Similarly, the "catalytic potentials" defined in figure 1 are not the true reduction potentials of the active site[9]. In the particular case of hydrogenase, the latter may also be distinct from the potentials measured in titration experiments, which are unlikely to be conducted under true equilibrium conditions: the most reduced state of hydrogenase cannot be produced under equilibrium conditions (unless  $E=E_{\text{eq}}$ , which, at low potential, would require a ten fold increase in  $H_2$  pressure every 30 mV down, see eq 1), because the substrate proton cannot be removed from the medium, as pointed out early on in the literature [33,34]. The situation is the same, on the opposite side of the redox scale, for the most oxidized state of the  $O_2$ -evolving Mn cluster of Photosystem II.

Our ultimate goal is to apply this strategy to hydrogenases experimental data, to find out what differences between homologous hydrogenases make their catalytic responses distinct, and in particular what makes some hydrogenases (like *Tam HydS*) behave "irreversibly" [25], in contrast to prototypical hydrogenases. In this ongoing work, an additional complication is that the above assumption of bimolecular protonation kinetics is not appropriate to describe the protonation of a buried active site. If a residue whose acidity constant is  $K_{\text{relay}}$  serves as a relay to transfer protons to and from a buried active site, the protonation and deprotonation rate constants  $k_+$  and  $k_-$ , respectively, depend on pH as follows [35]:

$$k_+ = \frac{k_+^{\text{max}}}{1 + \frac{K_{\text{relay}}}{[\text{H}^+]}} \quad (20)$$

$$k_- = \frac{k_-^{\text{max}}}{1 + \frac{[\text{H}^+]}{K_{\text{relay}}}} \quad (21)$$

The resulting equations of the catalytic potentials and limiting currents are more complex than those shown in this paper, and the electrochemical data alone can be used to identify the "best" model and determine all the corresponding parameters. However, the models could be useful on condition that the information from the electrochemical data is combined with the information obtained from redox titrations of the hydrogenase active site : the value of  $K$ , the acidity constant of the half reduced form of the active site, has been obtained in the case of various FeFe hydrogenases [32,36] and will have to be combined with electrochemical data to understand the catalytic properties of these enzymes.

## Competing interests statement

The authors have no competing interests to declare.

## Acknowledgements

This work was funded by the CNRS and Aix Marseille University. The authors are part of the French Network of Bioinorganic Chemistry ([www.frenchbic.cnrs.fr](http://www.frenchbic.cnrs.fr)).

## Vitae



Dr Christophe Léger obtained his Ph.D. from the University of Bordeaux and was a postdoc in the group of Fraser Armstrong from 1999 to 2002. He is “Directeur de Recherche” at CNRS. His interests lie in kinetic and mechanistic studies of complex metalloenzymes.



Vincent Fourmond obtained his Ph.D. at the interface of physics and biology from Université Paris Diderot in 2007. He held postdoctoral positions first in the group of Christophe Léger in Marseille and then Vincent Artero in Grenoble, before coming back to Marseille as a permanent CNRS researcher in 2011. His research interests revolve around the use of kinetic techniques, principally protein film electrochemistry, to understand the mechanisms of metalloenzymes (hydrogenases, CO dehydrogenases, molybdenum enzymes), the development of methodological aspects of PFE, and the development and maintenance of the open source data analysis software QSoas.



Andrea Fasano obtained his BSc in 2017 in Biotechnology at the Alma Mater Studiorum university of Bologna and his MSc in Industrial Biotechnology at the University of Padua in 2019. The following year he started his Ph.D. at the University of Aix Marseille University, in the laboratory of Dr. Christophe Léger, which focuses on mechanistic and kinetic studies of different classes of FeFe and NiFe hydrogenases by Protein Film Electrochemistry.

## References

- [1] N. Elgrishi, K.J. Rountree, B.D. McCarthy, E.S. Rountree, T.T. Eisenhart, J.L. Dempsey, A Practical Beginner's Guide to Cyclic Voltammetry, *J. Chem. Educ.* 95 (2018) 197–206. doi:10.1021/acs.jchemed.7b00361.
- [2] J.-M. Savéant, C. Costentin, *Elements of Molecular and Biomolecular Electrochemistry: An Electrochemical Approach to Electron Transfer Chemistry*, John Wiley & Sons, 2019.
- [3] M. Meneghello, A. Uzel, M. Broc, R.R. Manuel, A. Magalon, C. Léger, I.A.C. Pereira, A. Walburger, V. Fourmond, Electrochemical Kinetics Support a Second Coordination Sphere Mechanism in Metal-Based

- Formate Dehydrogenase, *Angew. Chem. Int. Ed Engl.* 62 (2023) e202212224. doi:10.1002/anie.202212224.
- [4] D.W. Cunningham, J.M. Barlow, R.S. Velasquez, J. Yang, Reversible and Selective CO<sub>2</sub> to HCO<sub>2</sub><sup>-</sup> Electrocatalysis near the Thermodynamic Potential, *Angew. Chem. Int. Ed Engl.* 59 (2020) 4443–4447. doi:10.1002/anie.201913198.
- [5] M. Del Barrio, M. Sensi, C. Orain, C. Baffert, S. Dementin, V. Fourmond, C. Léger, Electrochemical Investigations of Hydrogenases and Other Enzymes That Produce and Use Solar Fuels, *Acc. Chem. Res.* 51 (2018) 769–777. doi:10.1021/acs.accounts.7b00622.
- [6] A. Dutta, A.M. Appel, W.J. Shaw, Designing electrochemically reversible H<sub>2</sub> oxidation and production catalysts, *Nature Reviews Chemistry.* 2 (2018) 244–252. doi:10.1038/s41570-018-0032-8.
- [7] B. Reuillard, C. Costentin, V. Artero, Deciphering reversible homogeneous catalysis of the electrochemical H<sub>2</sub> evolution and oxidation: Role of proton relays and local concentration effects, *Angewandte Chemie International Edition.* (2023). doi:10.1002/anie.202302779.
- [8] V. Fourmond, C. Baffert, K. Sybirna, T. Lautier, A. Abou Hamdan, S. Dementin, P. Soucaille, I. Meynial-Salles, H. Bottin, C. Léger, Steady-state catalytic wave-shapes for 2-electron reversible electrocatalysts and enzymes, *J. Am. Chem. Soc.* 135 (2013) 3926–3938. doi:10.1021/ja311607s.
- [9] V. Fourmond, E.S. Wiedner, W.J. Shaw, C. Léger, Understanding and Design of Bidirectional and Reversible Catalysts of Multielectron, Multistep Reactions, *J. Am. Chem. Soc.* 141 (2019) 11269–11285. doi:10.1021/jacs.9b04854.
- [10] C. Costentin, Molecular Catalysis of Electrochemical Reactions. Overpotential and Turnover Frequency: Unidirectional and Bidirectional Systems, *ACS Catal.* 11 (2021) 5678–5687. doi:10.1021/acscatal.1c00744.
- [11] A. Molina, J. González, E. Laborda, Applicability of conventional protocols for benchmarking of unidirectional and bidirectional multi-electron homogeneous molecular catalysts beyond the pure kinetic regime, *Electrochim. Acta.* 428 (2022) 140934. doi:10.1016/j.electacta.2022.140934.
- [12] E.S. Rountree, B.D. McCarthy, T.T. Eisenhart, J.L. Dempsey, Evaluation of homogeneous electrocatalysts by cyclic voltammetry, *Inorg. Chem.* 53 (2014) 9983–10002. doi:10.1021/ic500658x.
- [13] H. Tatsumi, K. Takagi, M. Fujita, K. Kano, T. Ikeda, Electrochemical study of reversible hydrogenase reaction of *Desulfovibrio vulgaris* cells with methyl viologen as an electron carrier, *Anal. Chem.* 71 (1999) 1753–1759. doi:10.1021/ac981003l.
- [14] J.-M. Savéant, Molecular Catalysis of Electrochemical Reactions. Cyclic Voltammetry of Systems Approaching Reversibility, *ACS Catal.* 8 (2018) 7608–7611. doi:10.1021/acscatal.8b02007.
- [15] S.V. Hexter, F. Grey, T. Happe, V. Climent, F.A. Armstrong, Electrocatalytic mechanism of reversible hydrogen cycling by enzymes and distinctions between the major classes of hydrogenases, *Proc. Natl. Acad. Sci. U. S. A.* 109 (2012) 11516–11521. doi:10.1073/pnas.1204770109.
- [16] K. Sakai, B.-C. Hsieh, A. Maruyama, Y. Kitazumi, O. Shirai, K. Kano, Interconversion between formate and hydrogen carbonate by tungsten-containing formate dehydrogenase-catalyzed mediated bioelectrocatalysis, *Sensing and Bio-Sensing Research.* 5 (2015) 90–96. doi:10.1016/j.sbsr.2015.07.008.
- [17] S. Hardt, S. Stapf, D.T. Filmon, J.A. Birrell, O. Rüdiger, V. Fourmond, C. Léger, N. Plumeré, Reversible H<sub>2</sub> oxidation and evolution by hydrogenase embedded in a redox polymer film, *Nature Catalysis.* 4 (2021) 251–258. doi:10.1038/s41929-021-00586-1.
- [18] V. Fourmond, N. Plumeré, C. Léger, Reversible catalysis, *Nature Reviews Chemistry.* 5 (2021) 348–360. doi:10.1038/s41570-021-00268-3.
- [19] A. Abou Hamdan, S. Dementin, P.-P. Liebgott, O. Gutierrez-Sanz, P. Richaud, A.L. De Lacey, M. Rousset, P. Bertrand, L. Cournac, C. Léger, Understanding and tuning the catalytic bias of hydrogenase, *JACS.* 134 (2012) 8368–8371. doi:10.1021/ja301802r.
- [20] D.W. Mulder, J.W. Peters, S. Raugei, Catalytic bias in oxidation-reduction catalysis, *Chem. Commun.* . 57 (2021) 713–720. doi:10.1039/d0cc07062a.
- [21] H.R. Pershad, J.L. Duff, H.A. Heering, E.C. Duin, S.P. Albracht, F.A. Armstrong, Catalytic electron transport in *Chromatium vinosum* [NiFe]-hydrogenase: application of voltammetry in detecting redox-active centers and establishing that hydrogen oxidation is very fast even at potentials close to the reversible H<sup>+</sup>/H<sub>2</sub> value, *Biochemistry.* 38 (1999) 8992–8999. doi:10.1021/bi990108v.
- [22] C. Hessin, J. Schleinitz, N. Le Breton, S. Choua, L. Grimaud, V. Fourmond, M. Desage-El Murr, C. Léger, Assessing the Extent of Potential Inversion by Cyclic Voltammetry: Theory, Pitfalls, and Application to a Nickel Complex with Redox-Active Iminosemiquinone Ligands, *Inorg. Chem.* 62 (2023) 3321–3332. doi:10.1021/acs.inorgchem.2c04365.
- [23] C. Léger, A.K. Jones, S.P.J. Albracht, F.A. Armstrong, Effect of a Dispersion of Interfacial Electron Transfer Rates on Steady State Catalytic Electron Transport in [NiFe]-hydrogenase and Other Enzymes, *J. Phys. Chem. B.* 106 (2002) 13058–13063. doi:10.1021/jp0265687.

- [24] V. Fourmond, C. Léger, Modelling the voltammetry of adsorbed enzymes and molecular catalysts, *Current Opinion in Electrochemistry*. 1 (2017) 110–120. doi:10.1016/j.coelec.2016.11.002.
- [25] A. Fasano, H. Land, V. Fourmond, G. Berggren, C. Léger, Reversible or Irreversible Catalysis of H<sup>+</sup>/H<sub>2</sub> Conversion by FeFe Hydrogenases, *J. Am. Chem. Soc.* 143 (2021) 20320–20325. doi:10.1021/jacs.1c09554.
- [26] M. Sensi, M. del Barrio, C. Baffert, V. Fourmond, C. Léger, New perspectives in hydrogenase direct electrochemistry, *Current Opinion in Electrochemistry*. 5 (2017) 135–145. doi:10.1016/j.coelec.2017.08.005.
- [27] C. Costentin, Proton-Coupled Electron Transfer Catalyst: Homogeneous Catalysis. Application to the Catalysis of Electrochemical Alcohol Oxidation in Water, (2020). doi:10.1021/acscatal.0c01195.
- [28] C. Costentin, Electrochemical approach to the mechanistic study of proton-coupled electron transfer, *Chem. Rev.* 108 (2008) 2145–2179. doi:10.1021/cr068065t.
- [29] A. Fersht, University Alan Fersht, Structure and Mechanism in Protein Science: A Guide to Enzyme Catalysis and Protein Folding, W. H. Freeman, 1999. [https://play.google.com/store/books/details?id=QdpZz\\_ahA5UC](https://play.google.com/store/books/details?id=QdpZz_ahA5UC).
- [30] A. Cornish-Bowden, Fundamentals of Enzyme Kinetics (English Edition), 4th ed., Wiley-Blackwell, 2013.
- [31] J.A. Birrell, P. Rodríguez-Maciá, A. Hery-Barranco, A Beginner's Guide to Thermodynamic Modelling of [FeFe] Hydrogenase, *Catalysts*. 11 (2021) 238. doi:10.3390/catal11020238.
- [32] C. Sommer, A. Adamska-Venkatesh, K. Pawlak, J.A. Birrell, O. Rüdiger, E.J. Reijerse, W. Lubitz, Proton Coupled Electronic Rearrangement within the H-Cluster as an Essential Step in the Catalytic Cycle of [FeFe] Hydrogenases, *J. Am. Chem. Soc.* 139 (2017) 1440–1443. doi:10.1021/jacs.6b12636.
- [33] A.J. Pierik, W.R. Hagen, J.S. Redeker, R.B. Wolbert, M. Boersma, M.F. Verhagen, H.J. Grande, C. Veeger, P.H. Mutsaers, R.H. Sands, Redox properties of the iron-sulfur clusters in activated Fe-hydrogenase from *Desulfovibrio vulgaris* (Hildenborough), *Eur. J. Biochem.* 209 (1992) 63–72. doi:10.1111/j.1432-1033.1992.tb17261.x.
- [34] C. Léger, A.K. Jones, W. Roseboom, S.P.J. Albracht, F.A. Armstrong, Enzyme electrokinetics: hydrogen evolution and oxidation by *Allochromatium vinosum* [NiFe]-hydrogenase, *Biochemistry*. 41 (2002) 15736–15746. doi:10.1021/bi026586e.
- [35] J. Hirst, J.L.C. Duff, G.N.L. Jameson, M.A. Kemper, B.K. Burgess, F.A. Armstrong, Kinetics and Mechanism of Redox-Coupled, Long-Range Proton Transfer in an Iron–Sulfur Protein. Investigation by Fast-Scan Protein-Film Voltammetry, *J. Am. Chem. Soc.* 120 (1998) 7085–7094. doi:10.1021/ja980380c.
- [36] N. Chongdar, J.A. Birrell, K. Pawlak, C. Sommer, E.J. Reijerse, O. Rüdiger, W. Lubitz, H. Ogata, Unique Spectroscopic Properties of the H-Cluster in a Putative Sensory [FeFe] Hydrogenase, *J. Am. Chem. Soc.* 140 (2018) 1057–1068. doi:10.1021/jacs.7b11287.

# Kinetic modeling of $2e^-/1H^+$ and $2e^-/2H^+$ bidirectional catalytic cycles

## Supplementary Information

Andrea Fasano, Vincent Fourmond and Christophe Léger\*

Laboratoire de Bioénergétique et Ingénierie des Protéines, CNRS, Aix Marseille Université, Marseille, France.

Complete derivation of the pH dependence of  $E_{cat}^{ox}$  for the  $2e^-/2H^+$  case 5, in which the first redox step is coupled to fast protonation, while the second protonation occurs coupled to the second chemical step.

Eq 1 in the main text is here rewritten as:

$$E_{cat}^{ox} = E_1^0 - A$$

in which  $E_1^0$  depend on pH, and will be therefore  $E_1^{0'}$ , and A is defined as follow:

$$E_{cat}^{ox} = E_1^{0'} - A$$

$$A = -\frac{RT}{F} \ln \frac{k_2 + k_{-1} + k_{-2}}{k_2 + k_{-1}}$$

$E_1^{0'}$  and  $k_2$  depend on pH as follows:

$$E_1^{0'} = E_1^0 - 2.3 \frac{RT}{F} \times pH$$

$$k_2 = k_2' \times [H^+]$$

Substituting  $k_2$  into A gives:

$$A = -\frac{RT}{F} \ln \frac{k_2' \times [H^+] + k_{-1} + k_{-2}}{k_2' \times [H^+] + k_{-1}}$$

Dividing numerator and denominator by  $k_2 + k_{-1}$ , it becomes:

$$A = -\frac{RT}{F} \ln \frac{\frac{k_2' \times [H^+] + k_{-1} + k_{-2}}{k_{-1} + k_{-2}}}{\frac{k_2' \times [H^+] + k_{-1}}{k_{-1} + k_{-2}}}$$

After simplification one can multiply both denominator and numerator by the reciprocal of the second term of the sum at the denominator:

$$A = -\frac{RT}{F} \ln \frac{\left(1 + \frac{k'_2 \times [H^+]}{k_{-1} + k_{-2}}\right) \times \frac{k_{-2} + k_{-1}}{k_{-1}}}{\left(\frac{k'_2 \times [H^+]}{k_{-1} + k_{-2}} + \frac{k_{-1}}{k_{-2} + k_{-1}}\right) \times \frac{k_{-2} + k_{-1}}{k_{-1}}}$$

The denominator can now be simplified while the second term of the multiplication at the numerator can become the argument of a second logarithm:

$$A = -\frac{RT}{F} \left[ \ln \frac{1 + \frac{k'_2 \times [H^+]}{k_{-1} + k_{-2}}}{1 + \frac{k'_2 \times [H^+]}{k_{-1}}} + \ln \frac{k_{-2} + k_{-1}}{k_{-1}} \right]$$

Now, the rate constants that are dependent on proton concentration can be grouped:

$$A = -\frac{RT}{F} \ln \frac{1 + \frac{[H^+]}{K_b}}{1 + \frac{[H^+]}{K_e}} - \frac{RT}{F} \ln \frac{k_{-2} + k_{-1}}{k_{-1}}$$

Finally,  $E_1^{o'}$  and A can be substituted into the definition of  $E_{\text{cat}}^{\text{ox}}$  given at the beginning, to obtain:

$$E_{\text{cat}}^{\text{ox}} = E_1^0 - \frac{RT}{F} \ln(10) \times pH + \frac{RT}{F} \ln \frac{1 + \frac{[H^+]}{K_e}}{1 + \frac{[H^+]}{K_b}} + \frac{RT}{F} \ln \frac{K_e}{K_b}$$

where

$$K_e = \frac{k_{-1}}{k'_2}$$

$$K_b = \frac{k_{-1} + k_{-2}}{k'_2}$$

The same reasoning has been used to calculate  $E_{\text{cat}}^{\text{red}}$ ,  $i_{\text{lim}}^{\text{ox}}$ ,  $i_{\text{lim}}^{\text{red}}$  and for all the other cases described in the paper.